Sensors & Diagnostics

PAPER

View Article Online
View Journal | View Issue

Cite this: *Sens. Diagn.*, 2026, **5**, 739

Quantification of avian influenza A virus (H5N1) *via* enzymatic reactions and glucometer test strips

Md Reazul Islam, [a] Faisal Hossain, [a] Michael A. Joyce, [bc] Mohamed Elaish, [de] D. Lorne Tyrrell, [bc] Tom C. Hobman[bcd] and Michael J. Serpe *[a]

A sensor capable of quantifying avian influenza A virus (subtype H5) was developed by targeting hemagglutinin (HA) protein. This was accomplished by designing a solution-based sandwich assay that generated orthophosphate (PO_4^{3-}) in proportion to the concentration of HA protein (and hence virus particles) present in a sample. Virus particles were captured and concentrated using an H5-specific primary antibody conjugated to magnetic microparticles. Following magnetic separation, an alkaline phosphatase (AP)-conjugated secondary antibody was introduced to bind to the captured virus. The resulting assembly was exposed to *p*-nitrophenyl phosphate (PNPP), producing PO_4^{3-} in proportion to the amount of virus present. The generated phosphate was subsequently converted to glucose through the addition of maltose and maltose phosphorylase, and the resulting glucose was quantified amperometrically using an off-the-shelf commercial glucose test strip interfaced with a mini-potentiostat. Using this approach, limits of detection of 7.78×10^5 RNA copies per mL in binding buffer, 1.46×10^6 RNA copies per mL in artificial saliva, and 1.26×10^6 RNA copies per mL in tap water were obtained. Selectivity was demonstrated against respiratory pathogen pools, representative Gram-positive and Gram-negative bacteria, and severe acute respiratory syndrome coronavirus 2 (SARS-CoV-2). This work presents a modular immunoassay-based strategy that leverages widely available glucose test strips for quantitative viral detection in a laboratory proof-of-concept format and may be adaptable to other targets through substitution of capture and detection antibodies.

Received 7th January 2026,
Accepted 16th March 2026

DOI: 10.1039/d6sd00003g

rsc.li/sensors

Introduction

Avian influenza, commonly known as bird flu, is an infectious disease caused by different variants of avian influenza viruses (AIVs).[1] Influenza viruses types A, B, and C are the three major genera within the family *Orthomyxoviridae*, a group of single-stranded negative-sense RNA viruses with a segmented genome. Type A viruses are mostly responsible for avian influenza epidemics and pandemics.[2] AIVs pose global challenges due to their widespread circulation and the potential for high mortality in outbreaks caused by highly pathogenic strains.[3] To date, 18 hemagglutinin (HA; H1–H18) and 11 neuraminidase (NA; N1–N11) subtypes have been identified for influenza type A viruses, and different HA–NA combinations give rise to the various subtypes (*e.g.*, H5N1 and H7N9).[4] Since 1889, seroepidemiologic and virologic studies have shown that pandemics were caused by H1, H2, and H3 subtypes of influenza A viruses.[2] However, H5N1 is a highly pathogenic avian influenza strain that originated in southern China in the mid-1990s and has since caused recurrent outbreaks of avian influenza, with recent spillover events renewing concerns about potential transmission to humans.[5] Migratory birds and poultry trade are believed to play major roles in the global spread of H5N1 in poultry. As of January 2026, the World Health Organization (WHO) has documented 993 cases of highly pathogenic avian influenza (HPAI) caused by H5N1 infection in humans and 477 (48.0%) fatalities in 25 countries.[6] Recent outbreaks in wild birds, domestic birds, sea lions, and minks, together with ongoing genetic variation among HPAI H5N1 strains and increasing spillover into mammalian hosts, have raised concerns about potential transmission and public health risks.[3] This HPAI H5N1 lineage can be traced back to the original strain A/goose/Guangdong/1/96.[7] Recent epidemiological analyses have documented sporadic human infections associated with highly pathogenic H5N1 outbreaks, underscoring continued

[a] *Department of Chemistry, University of Alberta, Edmonton, AB, T6G 2G2, Canada. E-mail: serpe@ualberta.ca*
[b] *Dept. of Medical Microbiology and Immunology, University of Alberta, Edmonton, AB, Canada T6G 2S2*
[c] *Li Ka Shing Centre for Health Research Innovation, 7-126, Edmonton, AB T6G 2E1, Canada*
[d] *Department of Cell Biology, University of Alberta, Edmonton, AB T6G 2H7, Canada*
[e] *Poultry Disease Department, Faculty of Veterinary Medicine, Cairo University, Giza, Egypt*

zoonotic risk.[7] Therefore, the importance of developing sensors to detect and quantify this virus cannot be overlooked.

There are several methods to detect and quantify H5N1 virus and/or antibodies. Hemagglutination and hemagglutination inhibition (HI) assays represent two of the most widely employed serological methods for the diagnosis and surveillance of influenza, although additional serological approaches are also utilized. Wiriyarat *et al.* reported that red blood cells collected from goose and guinea pig had the highest hemagglutinin titres among the 5 species tested.[8] Hemagglutination and HI assays are highly sensitive and specific, and are considered the gold standard for the detection of antibodies against AIV.[9] However, when it comes to detection of H5N1 AIV in human serum, it has low sensitivity.[10] Another widely used method for AIV detection is enzyme-linked immunosorbent assay (ELISA). Different types of ELISA such as indirect ELISA, competitive ELISA (CELISA), and double antibody sandwich ELISA (DAS-ELISA) have been developed for this purpose.[11] In one example, CELISA utilized recombinant baculovirus vector '*autographa californica* nuclear polyhedrosis' virus, expressing the nucleoprotein (NP) gene of A/Ann Arbor/6/60 type influenza A virus for the serological diagnosis of AIV exposure in birds.[12] Zhang *et al.* used monoclonal antibodies to capture AIV nucleocapsids and anti-NP horseradish peroxidase-conjugated rabbit polyclonal immunoglobulin G (IgG) as detection antibodies.[13] Since, both the antibodies were designed to bind the NP in a sandwich orientation, this method was named "double antibody sandwich enzyme-linked immunosorbent assay" (DAS-ELISA). The authors reported the LOD of their method to be 2.5 ng of NP. The DAS-ELISA method can detect different variants of AIV with high sensitivity and specificity, but was reported to have poor reproducibility.[14] Polymerase chain reaction (PCR) and real time PCR (RT-PCR) are widely used and accepted techniques for detection and quantification of microorganisms by leveraging the nucleotide sequence of the target organism.[15] RT-PCR is the gold standard when it comes to detection and quantification of AIV RNA during active infection.[16] In one study, Chen *et al.* used universal primers that were designed for the HA gene and achieved higher accuracy than routine RT-PCR studies.[17] RT-PCR is reported to have higher sensitivity compared to ELISA and is more efficient and less time-consuming than virus isolation and identification-based detection methods. Despite its high sensitivity and specificity, the performance of quantitative RT-PCR can be affected by factors such as the presence of inhibitors in the sample matrix, inefficient RNA extraction, and degradation of RNA prior to analysis. Moreover, its reliability depends heavily on stringent operational standards and well-maintained equipment, making it susceptible to false positives or negatives in suboptimal testing environments.[11] These limitations highlight the need for alternative diagnostic strategies that may complement existing methods in settings where simplified or amplification-free detection is desirable.

For decades, personal glucometers (PGM) have been used by many millions of people worldwide on a daily basis to manage diabetes.[18] Because of its widespread availability, facile operation and cost effectiveness, PGMs have also been utilized to detect various non-glucose analytes such as inorganic ions (lead[19] and phosphate[20]), small molecules (ATP and cocaine[21]), or biological targets (virus[22] and bacteria[23]). A glucometer consists of an electronic readout device connected to a test strip, which contains glucose dehydrogenase and other mediators, and generates an electrical signal that can be predicted from the Cottrell equation (eqn (1)):[24]

$$i = (nFAD^{1/2}C)/(\pi t)^{1/2} \quad (1)$$

where n = number of electrons, F = Faraday constant, A = area of the electrode, D = diffusion coefficient of the mediator, C = initial analyte concentration, and t = time.

Glucose test strips are highly selective, and sensitive, and only require small volumes of sample (<1 μL) to generate a response.[24] Recently, our group developed a sensor to quantify orthophosphate (PO_4^{3-}) in water utilizing a glucometer test strip. In this study, Hossain *et al.* utilized the enzymatic cleavage of maltose in the presence of PO_4^{3-} and maltose phosphorylase (MP) to generate an equivalent amount of glucose that could be quantified using a glucometer test strip and a mini potentiostat.[20] In another study, a glucometer test strip was used to detect and quantify SARS-CoV-2 antibody and virus in physiologically relevant matrices.[22] The SARS-CoV-2 study was performed using a process similar to DAS-ELISA where multiple antibodies and enzymatic reactions were used to generate an amount of glucose that corresponded to the concentration of the target analyte. The use of a highly sensitive mini-potentiostat played a vital role in the above examples as the consumer electronics that are typically sold with these strips are not sensitive enough for our application, *i.e.*, they exhibit a limit of detection (LOD) of ~600 μM glucose. The mini-potentiostat used here with the glucose test strips exhibited an LOD of 1.45 μM of glucose in complex matrices.[20]

In this submission, we report the development of a sensor system that combines a commercial glucose test strip with a custom potentiostat-based reader to improve upon the detection capabilities of a standard glucometer. The system was optimized to detect and quantify the H5N1 variant of avian influenza virus (AIV) by specifically targeting the H5 HA protein. The assay targets HA, the major viral surface glycoprotein responsible for host cell entry, in a sandwich antibody format, with enzymatic signal generation converted to glucose. The glucose test strip transduces this chemical signal into an electrical current, which is then read out with enhanced sensitivity by our potentiostat.[22] Selectivity was determined using common interferents, and the assay performed reliably in both saliva and tap water, representing

physiologically and environmentally relevant matrices. Using this configuration, a LOD of 7.78×10^5 RNA copies per mL was achieved for intact H5N1 virus particles within the tested concentration range. As analytical sensitivity varies substantially across assay formats and reporting units, direct numerical comparison between platforms should be interpreted cautiously. A detailed performance comparison with recent representative H5/H5N1 detection platforms is provided in Table S1 of SI, including analytical limits of detection, assay formats, and sample matrices as reported in the literature. Although H5N1 is emphasized here due to its current impact on poultry and human health, the modular assay design allows substitution of capture and detection antibodies, enabling straightforward adaptation to other pathogens or small-molecule targets without altering the basic workflow.

Materials and methods

Materials

Avian influenza H5N1 HA recombinant rabbit monoclonal antibody specific to the HA protein of H5N1 AIV, influenza H5N1 HA (A/Vietnam/1194/2004) polyclonal antibody, Dynabeads M280 streptavidin, and a DynaMag™-2 magnet were purchased from Thermo Fisher Scientific (Waltham, Massachusetts). Influenza A [A/Hong Kong/483/97 (H5N1)] hemagglutinin (HA) protein was purchased from ACROBiosystems (Newark, DE). Biotinylation Kit/Biotin conjugation kit (fast, type B)–Lightning-Link®, alkaline phosphatase (AP) conjugation kit–Lightning-Link®, and FITC conjugation kit (fast)–Lightning-Link® were purchased from Abcam (Toronto, Ontario). The AP yellow liquid substrate system for ELISA *para*-nitrophenyl phosphate (PNPP), D-maltose monohydrate, Tween 20, Tris-base and potassium chloride (KCl) (ACS reagent, 99.0–100.5%), artificial saliva for pharmaceutical research, Amicon® Ultra centrifugal filter, 10 kDa MWCO for concentration and purification, Madin–Darby Canine Kidney Cell (MDCK) from ATCC (CCL-34), Dulbecco's Modified Eagle's Medium (DMEM), trypsin (TPCK treated), and penicillin–streptomycin were purchased from Millipore Sigma (Oakville, Ontario). Recombinant maltose phosphorylase from *E. coli* (1000 units) was purchased from Creative Enzymes (Shirley, NY). HEPES (*N*-2-hydroxyethylpiperazine-*N*′-2-ethanesulfonic acid) buffer (1 M, 0.2 μm filtered) and beta propiolactone (BPL) for H5N1 inactivation, concentrated hydrochloric acid (HCl), and bovine serum albumin (BSA) were purchased from Sigma Aldrich (Oakville, Ontario). NATtrol Respiratory Verification Panel and mixed titre bacteria were from ZeptoMetrix (Buffalo, NY). Accu-Chek Guide test strips were purchased from a local pharmacy. The potentiostat was from Biodevice Technology Ltd. (Ishikawa, Japan). An Olympus 1X71 inverted optical/fluorescence microscope was used to conduct fluorescence imaging experiments. An Allegra X-30R centrifuge from Beckman Coulter was used to concentrate the virus suspension. All virus and bacterial experiments were conducted in separate biosafety level 2 (BSL-2) facilities of biological services of Dept. of Chemistry, University of Alberta. Milli-Q-grade water (18.2 MΩ cm) from a Millipore Milli-Q-Plus system (Billerica, Massachusetts) was used in all experiments unless mentioned otherwise. UV-vis absorbance was measured at 405 nm using a Hewlett–Packard Agilent 8453 UV-vis spectrophotometer equipped with an 89090A temperature controller. All chemical structures were drawn using Chemdraw and figures were created with https://BioRender.com.

Propagation and inactivation of H5N1 virus

Virus propagation and inactivation were performed according to a published protocol with minor modifications when necessary.[25] A 6 : 2 reassortment influenza virus containing the hemagglutinin (HA) and neuraminidase (NA) genes from A/Vietnam/1194/2004 (H5N1) and the six internal genes from A/Puerto Rico/8/34 (PR8) strain was a kind gift from Matthew Miller (McMaster University). The virus was propagated in MDCK cells at a multiplicity of infection (MOI) of 0.01. The virus was incubated for 1 h at 37 °C in DMEM supplemented with 1 μg mL^{-1} TPCK-treated trypsin to facilitate viral entry. Following incubation, the medium was removed, and the cells were washed with phosphate-buffered saline (PBS). The medium was then replaced with DMEM containing 1 μg mL^{-1} TPCK trypsin, 100 IU mL^{-1} penicillin, and 100 μg mL^{-1} streptomycin, and the infection was allowed to proceed for 72 h. The virus-containing supernatant was collected and inactivated by treatment with BPL at a ratio of 1 : 1000 (v/v, BPL : virus). The mixture was incubated overnight at 4 °C to ensure complete viral inactivation while maintaining the structural integrity of viral proteins. The overall workflow from virus preparation to electrochemical detection is illustrated in Scheme 1. All the proteins, antibodies, and virus solutions were diluted in binding buffer (0.01 M Tris, 150 mM KCl, 0.1% Tween 20, 0.1% BSA, pH 7.4), except for MP and maltose that were prepared in 0.1 M HEPES buffer (pH 5.2).

Conjugation of the anti H5N1 monoclonal antibody to the magnetic particle (step 1, Scheme 1)

First anti-H5N1 monoclonal antibodies were biotinylated using a biotinylation kit following the manufacturer's protocol. Then biotinylated antibodies were conjugated to streptavidin coated magnetic particles (10 μL, 10 mg mL^{-1}): the magnetic particles were first washed with 200 μL of wash buffer (0.01 M Tris, 150 mM KCl, 0.1% Tween 20) in an Eppendorf tube by vortex mixing for 30 s, followed by sedimentation with a DynaMag™-2 for 2 min and the supernatant was removed. The washed particles were then incubated with the biotinylated H5N1 antibody (50 μL, 10 μg mL^{-1}) for 1 h at room temperature (rt). Unbound protein was then removed by washing the modified magnetic particles as before.

Conjugation of HA protein or H5N1 AIV to the primary antibody modified magnetic particle (step 2, Scheme 1)

Primary antibody conjugated magnetic particles were incubated with HA protein or different amounts of virus

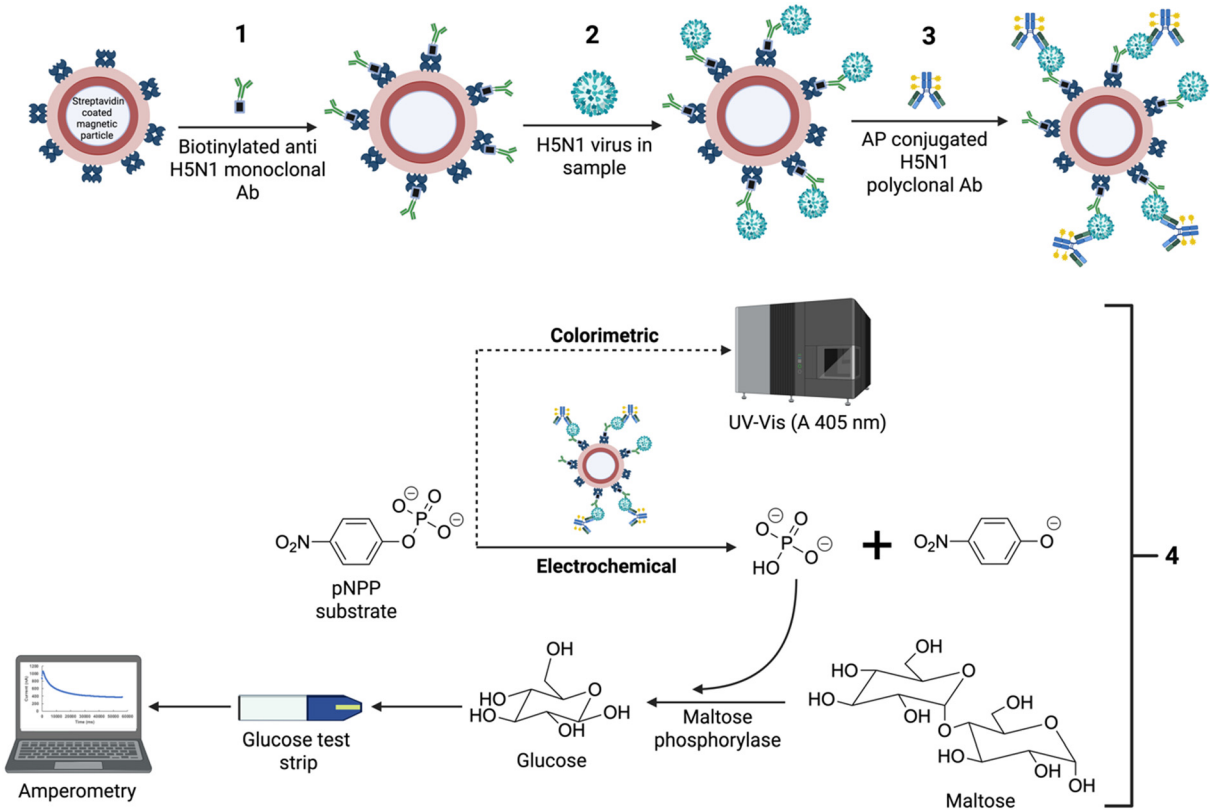

Scheme 1 Step by step process for H5N1 AIV quantification using the DAS-ELISA-based method with a glucometer test strip and potentiostat.

particles. 400 μL of HA protein or virus particles suspended in binding buffer or other matrices were conjugated with the magnetic particles for 15 min at rt and then washed 2×.

Binding of the alkaline phosphatase (AP) conjugated secondary antibody to the protein and/or virus modified magnetic particle (step 3, Scheme 1)

The anti-H5N1 polyclonal antibody was conjugated to AP using an AP conjugation kit following the manufacturer's protocol. Following HA binding to conjugated magnetic particles and washing, 200 μL of 2 μg mL^{-1} AP conjugated secondary antibody was incubated with the protein/virus modified magnetic particles for 15 min at rt. The particles were then washed 6×.

Detection of protein/virus (step 4, Scheme 1)

The washed particles from step 3 were exposed to 200 μL of 20% PNPP liquid substrate for 15 min at 37 °C to generate PO_4^{3-} in proportion to the captured HA protein and H5N1 AIV. The amount of generated PO_4^{3-} is therefore proportional to virus concentration.

To compare electrochemical readout with conventional ALP–PNPP colorimetric detection, the 200 μL PNPP reaction mixture was divided into two equal aliquots (100 μL each), and the resulting signals were evaluated using both detection modes (Table S2, SI). As can be seen from our data and supported by previous studies, electrochemical detection approaches often provide higher analytical sensitivity than absorbance-based colorimetric measurements due to lower background noise and efficient signal transduction.[26] One aliquot was transferred to a cuvette and the absorbance at 405 nm (A405) was measured using a UV–vis spectrophotometer. The second aliquot was processed for phosphate-to-glucose conversion and subsequent electrochemical quantification as described below.

To generate glucose in proportion to PO_4^{3-} produced by AP, 100 μL of the PNPP reaction solution was neutralized with 40 μL of 0.5 M HCl. Subsequently, 100 μL of the neutralized solution was combined with 5 μL of 100 mM maltose and maltose phosphorylase (20 U mL^{-1}) in 0.1 M HEPES buffer (pH 5.2) to obtain a final volume of 200 μL and incubated at 42 °C for 2 h 15 min. The reaction was terminated by placing the vial in a boiling water bath for 10 min to ensure complete and reproducible quenching of enzymatic activity, followed by centrifugation (2 min) and cooling (10 min).

The generated glucose was quantified using an Accu-Chek Guide test strip interfaced with a mini-potentiostat at 400 mV, consistent with previous reports.[22,27] The average current from 3–20 s of the chronoamperometric trace was used for analysis. All samples and blanks underwent identical capture, washing, substrate incubation, and enzymatic processing steps prior to signal measurement, and all data were normalized to identically processed reagent blanks. The limit of detection (LOD) was calculated as $(3\sigma_{blank})$/slope of the

calibration curve, where σ_{blank} represents the standard deviation of blank measurements (n = 3 strips). Error bars represent the standard deviation of three replicate measurements obtained using independent test strips.

Results and discussion

Optimization of the sensor

We initially optimized sensor performance using purified HA protein. First, the pH of the final reaction mixture was varied – 4.7, 5.2, 5.7, and 6.5 – and the relative current for 1 nM HA protein was highest at pH 5.2, with the volume of magnetic particles at 10 μL (10 mg mL^{-1}) and all other conditions, including primary and secondary antibody incubation times, held constant (Fig. 1A). Next, we optimized the volume of magnetic particles by testing 5, 10, and 15 μL (Fig. 1B) at pH 5.2. For 1 nM HA protein, the relative current nearly doubled when increasing the particle volume from 5 to 10 μL but showed no significant change between 10 and 15 μL. Therefore, a final reaction pH of 5.2 and a magnetic particle volume of 10 μL was selected for subsequent experiments. One of the most important criteria of our sensor was the attachment of antibodies for HA protein (analyte) to the magnetic particles *via* biotin–streptavidin conjugation. To validate this binding event, we labeled the secondary antibody with fluorescein isothiocyanate (FITC). After forming the magnetic particle-primary antibody-HA protein complex (1 nM), the FITC-labeled secondary antibody was added, incubated, and washed as described before. A control sample was processed in parallel without HA protein. We observed that the magnetic beads showed no detectable fluorescence in the absence of HA (Fig. 1C), whereas fluorescent magnetic particles were clearly observed when HA was present (Fig. 1D). The overall organization of the FITC-based imaging approach is illustrated in Fig. 1E.

Detection and quantification of H5N1 AIV

To determine the sensor's ability to quantify H5N1 AIV in different matrices, we measured the average current of the sensor when exposed to five different concentrations (RNA copies per mL) of H5N1 AIV. We tested the virus concentration ranging from 2.94×10^6 RNA copies per mL to 5.88×10^7 RNA copies per mL of H5N1 and calculated the average relative amperometric signal (compared to the reagent blank) between 3 and 20 s as a function of virus

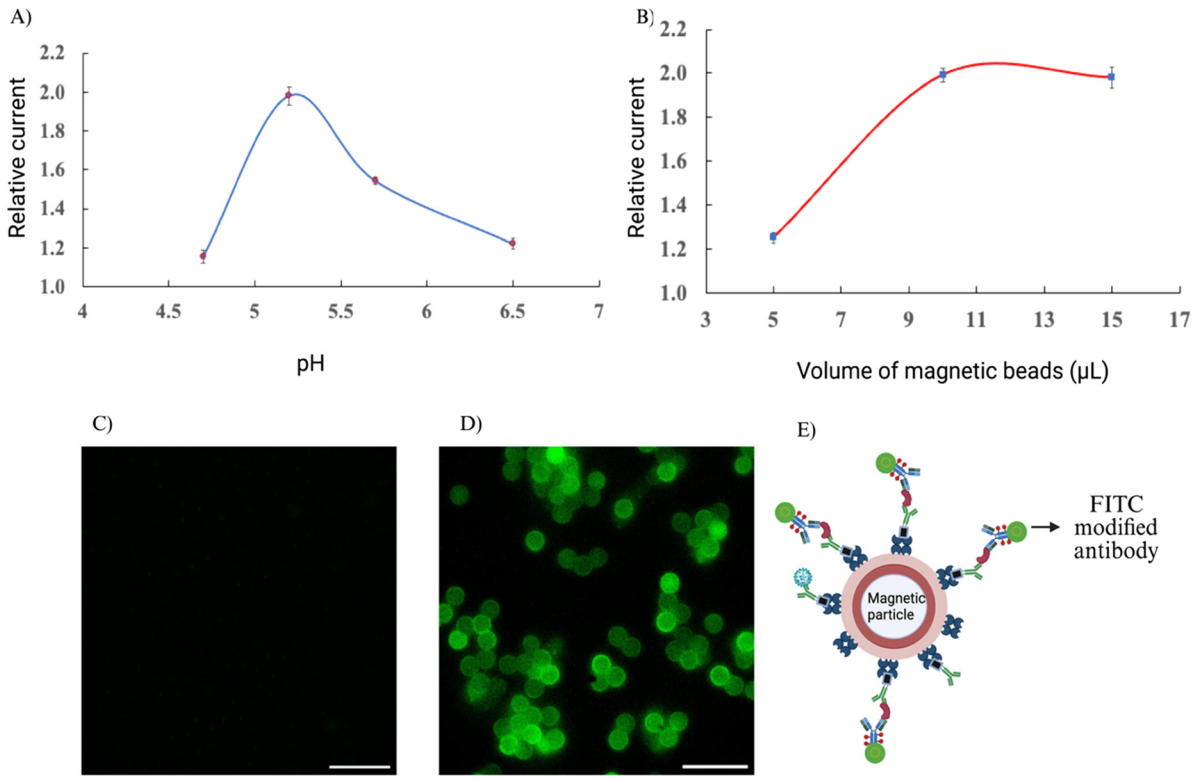

Fig. 1 Sensor optimization. (A) Relative current *vs.* pH of the final reaction. Relative current compared to the method blank is plotted against 4 different pH values of the final reaction (4.7, 5.2, 5.7, and 6.5). (B) Impact of the volume of magnetic particles used for antibody and analyte capture. Relative current compared to the method blank is plotted against the amounts of 3 different volumes of magnetic particles, 5 μL, 10 μL and 15 μL. For (A) and (B), each data point is the average of three replicate measurements using 3 different test strips and the error bar is the standard deviation of these 3 measurements. (C) and (D) Characterization of binding of antibodies and HA protein to magnetic beads. For the blank (C), where there was no HA protein, the FITC modified secondary antibody did not bind to the magnetic particles, so no fluorescence signal was found; however, in (D) when HA protein was present, we see clear fluorescence of FITC modified antibody after washing. Scale bar = 10 μm. (E) Cartoon representation of the assembly of the magnetic particle for fluorescence detection.

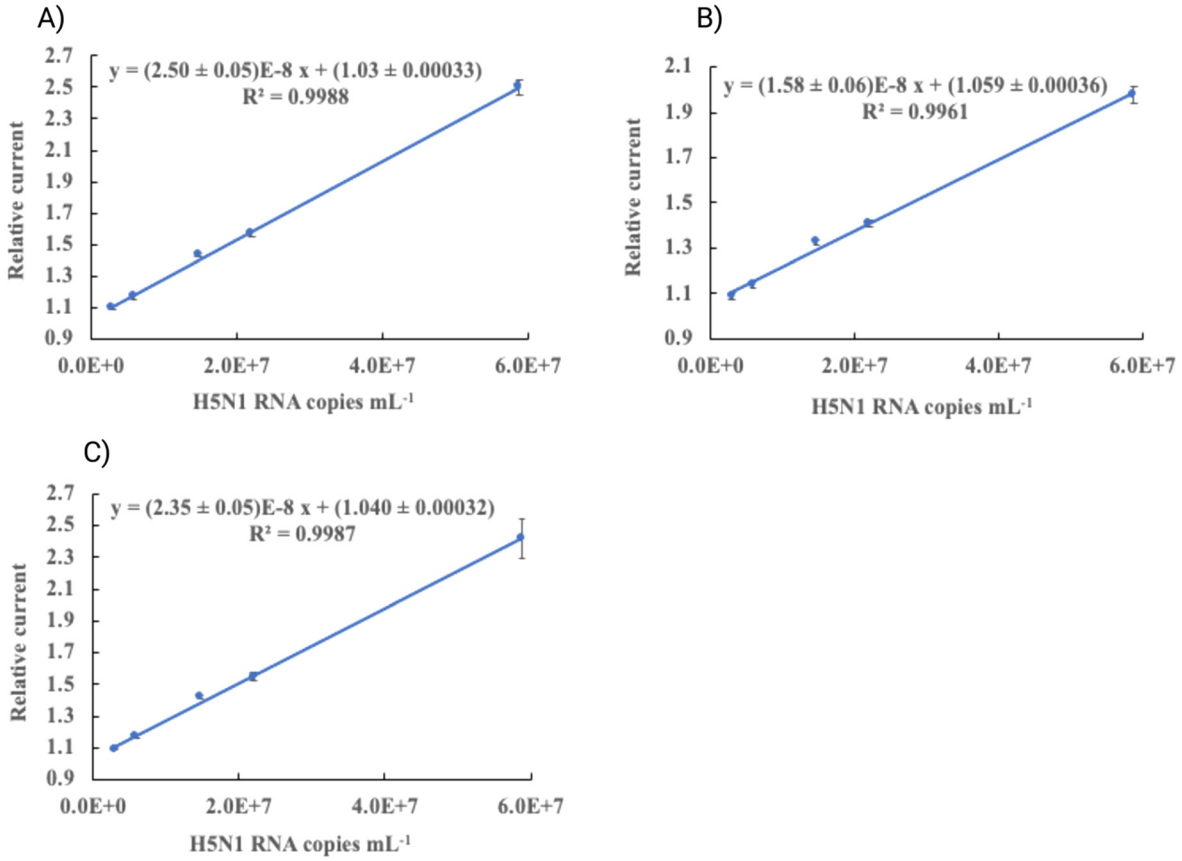

Fig. 2 Calibration curves for quantification of H5N1 AIV. (A) Calibration curve for H5N1 ranging from 2.94 × 10^6 to 5.88 × 10^7 RNA copies per mL in binding buffer. Each data point is the mean of relative current values for two separate days. (B) Calibration curve for the same viral concentration range in tap water as the matrix. (C) Calibration curve when artificial saliva was used as the matrix for viral suspension at the same particle concentrations. For panels B and C, each data point represents the average of three replicates using three different glucose test strips. Error bars represent the standard deviation of the measurements.

particle number. We observed the response to be linear across the tested range of virus concentrations, with regression coefficients (R^2) approaching 1 (Fig. 2A). We then determined our sensor performance in various matrices, *i.e.*, tap water and artificial saliva. The selected matrices were chosen based on prior literature and practical relevance. Leung *et al.* concluded that testing drinking water for poultry is an effective way for surveillance of avian influenza virus and this should be performed in influenza endemic regions.[28] Artificial saliva was used as a model complex biological matrix to evaluate assay robustness in protein-rich and ion-containing environments. Tap water was selected to represent environmental surveillance contexts relevant to poultry drinking water monitoring, as previously described.[28] These matrices were used to assess compatibility and matrix tolerance rather than to imply clinical specimen recommendations. Fig. 2B and C show the calibration curves when tap water and artificial saliva were used as matrices for the virus. Although city tap water may contain low levels of phosphate additives, the sample matrix is removed through repeated washing steps (8× washing with wash buffer between sample incubation and PNPP addition) prior to substrate addition. Consequently, endogenous phosphate is not expected to contribute directly to the measured electrochemical signal. In addition, the calibration behavior observed in tap water closely matched that obtained in binding buffer, further indicating that potential phosphate species present in the matrix do not measurably contribute to the electrochemical signal under the assay conditions. The slightly lower LOD in saliva and tap water can be attributed to the fact that both artificial saliva and tap water contain inorganic ions, which may influence antibody–antigen interactions through ionic strength effects.[29] The LOD values were 1.26 × 10^6 RNA copies per mL and 1.46 × 10^6 RNA copies per mL for tap water and saliva, respectively. These values demonstrate quantitative detection of intact virus within the tested concentration range across the evaluated matrices. Spike-recovery, accuracy, and precision analyses across all tested concentrations and matrices are summarized in Table S3 (SI), where intra and inter-assay coefficients of variation (CV%) and percent recoveries are reported to further support quantitative performance. Recovery values across matrices ranged from 33% to 120%, with lower recoveries at the lowest concentration in tap water likely reflecting matrix-associated antibody binding effects near the lower end of the calibration range rather than

systematic analytical bias. Such variability at concentrations approaching the limit of detection reflects the increased sensitivity of recovery calculations to small signal fluctuations at low analyte levels. This concentration corresponds to the lower end of the calibration range, where signal-to-noise effects are amplified, and recovery calculations become more sensitive to small absolute deviations.

It is recognized that certain electroactive compounds, including phenolic species, ascorbic acid, and uric acid, can interfere with some glucose strip formats. In the present assay, glucose is enzymatically generated only after antibody-mediated capture and multiple washing steps, which substantially reduces matrix carryover. Furthermore, electrochemical measurements were conducted under defined buffer conditions and normalized to identically processed blanks. Under the tested conditions, no evidence of matrix-derived electrochemical interference was observed. This observation is consistent with the findings reported by Hossain *et al.*, who similarly observed no significant interference when river water and tap water were used as matrices to evaluate assay robustness.[20] Nonetheless, evaluation in clinical specimens containing elevated endogenous electroactive species would be an important consideration in future validation studies.

Viral loads reported in infected hosts span a broad range depending on specimen type, disease stage, and host species. Published studies have documented high viral burdens in severe human cases;[30] however, reported viral levels and distribution can vary substantially across host species and biological contexts.[31] Accordingly, analytical sensitivity should be interpreted within the intended application framework. To contextualize the analytical performance of the present method, a comparison with representative H5/H5N1 detection platforms has been added (Table S1, SI). Recent studies report substantially lower numerical limits of detection, particularly for amplification-based molecular assays and certain electrochemical biosensors. The present work does not aim to replace nucleic acid amplification-based diagnostics in terms of analytical sensitivity, but instead demonstrates a modular enzymatic signal-transduction strategy for quantitative immunodetection of intact virus particles using commercially available components and electrochemical readout.

For laboratory validation, enzymatic reactions were terminated by brief boiling to ensure complete and reproducible quenching prior to electrochemical measurement. For translation toward field or on-farm applications, this step could be simplified through alternative engineering strategies, such as chemical quenching *via* rapid pH adjustment, timed

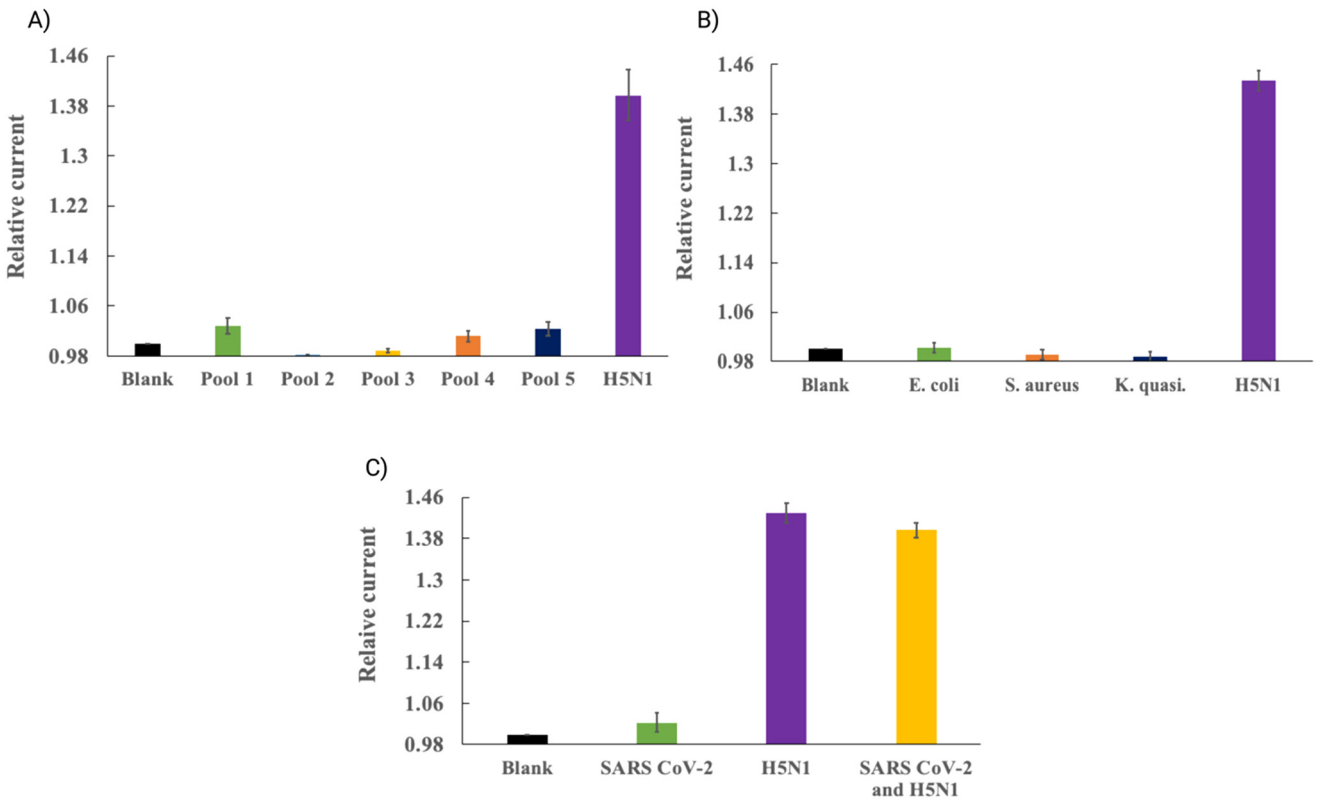

Fig. 3 Selectivity study of the H5N1 AIV sensor. (A) Comparison of response in relative current for H5N1 AIV against 5 respiratory pathogen pools. (B) H5N1 AIV *vs.* 3 other bacteria: *E. coli* = *Escherichia coli*, *S. aureus* = *Staphylococcus aureus*, *K. quasi.* = *Klebsiella quasipneumoniae*. (C) H5N1 and SARS-CoV-2 as separate and mixed virus titers. *Y* axis of all three plots represents the relative currents obtained from the amperometric signal compared to the reagent blank. Each bar is the average of 3 replicates with 3 different strips and the error bar is defined as the standard deviation of these three measurements.

reaction cartridges with pre-defined incubation windows, or enzyme immobilization/compartmentalization strategies, as widely discussed in enzyme immobilization and biocatalytic process design literature.[32]

Selectivity of H5N1 AIV detection

Since our device can quantify virus in different matrices, we investigated whether it can selectively detect the H5N1 AIV in the presence of other biologically relevant interfering pathogens. We chose three types of interference study where we tested our sensor's selectivity against 5 respiratory pathogen pools commercially obtained from ZeptoMatrix, 3 bacteria strains to cover Gram positive and negative spectra of bacteria and severe acute respiratory syndrome corona virus 2 (SARS-CoV-2). Fig. 3(A) shows the data for the selectivity study of H5N1 AIV compared to 5 different respiratory pathogen pools, where each pool contains at least 4 pathogens – a list of the specific pathogens in these pools are given in Table S4 of the SI. Each pool, and other interfering pathogens, were introduced into the sensor and relative currents obtained from the amperometric signal are plotted as described above. For bacteria, we chose *Escherichia coli* (*E. coli*, Gram negative), *Staphylococcus aureus* (Gram positive) and *Klebsiella quasipneumoniae* (Gram negative). As can be seen in Fig. 3(B), our devices selectively respond to H5N1, since the relative current for the 3 bacterial strains were almost same as that of the blank. To assess potential cross-reactivity with SARS-CoV-2, we evaluated our sensor response to SARS-CoV-2 and H5N1 individually, as well as to a mixture of both viruses at biologically relevant concentrations appropriate for each virus. We observed that the relative current for SARS-CoV-2 alone was comparable to the blank, but when mixed with H5N1, the current is almost at the same level as that of H5N1 alone. This shows our sensor's ability to selectively detect and quantify H5N1 AIV even with SARS-CoV-2 present in the same mixture, which can be useful for instances of co-infection. All interfering species were subjected to the same inactivation procedure used for H5N1. For H5N1, 1.47×10^7 RNA copies per mL were used and for SARS-CoV-2, 1.0×10^8 PFU per mL was chosen.

The specific pathogens and bacteria were selected based on their relevance to respiratory infections, environmental exposure, and clinically reported co-infection scenarios. Respiratory pathogen pools have previously been used as interfering species for influenza-causing viruses.[22,33] To assess environmental and bacterial interference, *E. coli* was included because it is commonly encountered in environments affected by fecal contamination.[34] Additional bacterial species relevant to influenza-associated co-infections were also evaluated. Rowe *et al.* demonstrated that influenza A virus infection increases adherence of *Staphylococcus aureus* to respiratory epithelial cells,[35] while *Klebsiella quasipneumoniae* has been identified as a common bacterial co-infection in both chickens[36] and hospitalized humans.[37] Finally, SARS-CoV-2 was included as a clinically relevant viral interferent due to its extensive study over the past five years, overlapping symptoms with H5N1, and reported co-infections that can exacerbate disease severity.[38] Collectively, these results demonstrate selective detection of H5N1 under the tested experimental conditions in the presence of representative respiratory pathogens and bacteria.

Since H5N1 AIV has attracted renewed attention due to spillover events in poultry[39] and dairy cattle[40] in North America, and for humans,[41] the developed platform represents an alternative electrochemical strategy for selective detection and quantification of this pathogen in the evaluated matrices.

Conclusion

We report a sensor platform utilizing a commercial glucometer test strip capable of quantifying H5N1 AIV in environmentally and physiologically relevant matrices. The platform demonstrated reproducible detection of H5N1 virus with a limit of detection of 7.78×10^5 RNA copies per mL in binding buffer across the tested concentration range. Moreover, the potential interfering pathogens had no significant interference with the sensor's detection. Finally, the modular design enables substitution of capture and detection antibodies, allowing extension of this enzymatic electrochemical strategy to other viral or protein targets following appropriate optimization.

Author contributions

Md Reazul Islam: conceptualization, methodology, investigation, data curation, formal analysis, visualization, writing – original draft, writing – review & editing. Faisal Hossain: conceptualization, methodology, investigation (fluorescence imaging). Michael A. Joyce: investigation (virus propagation and preparation), resources, writing – review & editing. Mohamed Elaish: investigation (virus propagation and preparation). D. Lorne Tyrrell: supervision, resources, writing – review & editing. Tom C. Hobman: supervision, resources, writing – review & editing. Michael J. Serpe: conceptualization, supervision, funding acquisition, project administration, writing – review & editing. All authors have read and agreed to the published version of the manuscript.

Conflicts of interest

There are no conflicts to declare.

Data availability

The datasets generated during and/or analysed during the current study are not publicly available due to potential patent filings, but are available from the authors on reasonable request.

Supplementary information (SI) is available. See DOI: https://doi.org/10.1039/d6sd00003g.

Acknowledgements

MJS acknowledges funding from the University of Alberta (the Department of Chemistry and the Faculty of Science), the Natural Sciences and Engineering Research Council of Canada (NSERC), the Canada Foundation for Innovation (CFI), the Alberta Advanced Education & Technology Small Equipment Grants Program (AET/SEGP), Grand Challenges Canada, Canadian Institutes of Health Research (Avian Influenza One Health Research Funding), Striving for Pandemic Preparedness–The Alberta Research Consortium (SPP–ARC), and the Canada Biomedical Research Fund and Biosciences Research Infrastructure Fund. The authors gratefully acknowledge Prof. Matthew Miller (McMaster University) and his group for the kind gift of 6.2 reassortment influenza virus. The authors acknowledge the use of ChatGPT (OpenAI) for assistance with language refinement and organization of contents. All scientific content, data, analysis, and conclusions were developed and verified by the authors.

References

1 N. Mittal and B. Medhi, *Int. J. Health Sci.*, 2007, **1**, 277–283.
2 S. S. Y. Wong and K. Yuen, *Chest*, 2006, **129**, 156–168.
3 J. Charostad, M. R. Z. Rukerd, S. Mahmoudvand, D. Bashash, S. M. A. Hashemi, M. Nakhaie and K. Zandi, *Travel Med. Infect. Dis.*, 2023, **55**, 102638.
4 R. Henry and F. A. Murphy, Etymologia: Hemagglutinin and Neuraminidase, *Emerging Infect. Dis.*, 2018, **24**(10), 1849, DOI: 10.3201/eid2410.et2410.
5 J. S. M. Peiris, M. D. de Jong and Y. Guan, *Clin. Microbiol. Rev.*, 2007, **20**, 243–267.
6 World Health Organization, Cumulative number of confirmed human cases for avian influenza A(H5N1) reported to WHO, 2003–2026, 20 February 2026, https://www.who.int, (accessed March 05, 2026).
7 F. Krammer and S. Schultz-Cherry, *Nat. Rev. Immunol.*, 2023, **23**, 267–268.
8 W. Wiriyarat, H. Lerdsamran, P. Pooruk, R. G. Webster, S. Louisirirotchanakul, P. Ratanakorn, K. Chaichoune, K. Nateerom and P. Puthavathana, *Vet. Microbiol.*, 2010, **146**, 346–349.
9 A. Comin, N. Toft, A. Stegeman, D. Klinkenberg and S. Marangon, *Influenza Other Respir. Viruses*, 2013, **7**, 257–264.
10 T. Rowe, R. A. Abernathy, J. Hu-Primmer, W. W. Thompson, X. Lu, W. Lim, K. Fukuda, N. J. Cox and J. M. Katz, *J. Clin. Microbiol.*, 1999, **37**, 937–943.
11 X. Fu, Q. Wang, B. Ma, B. Zhang, K. Sun, X. Yu, Z. Ye and M. Zhang, *Int. J. Mol. Sci.*, 2023, **24**, 17157.
12 A. L. Shafer, J. B. Katz and K. A. Eernisse, *Avian Dis.*, 1998, **42**, 28–34.
13 A. Zhang, M. Jin, F. F. Liu, X. Guo, Q. Hu, L. Han, Y. Tan and H. Chen, *Avian Dis.*, 2006, **50**, 325–330.
14 J. S. Ellis, D. M. Fleming and M. C. Zambon, *J. Clin. Microbiol.*, 1997, **35**, 2076–2082.
15 P. Kralik and M. Ricchi, *Front. Microbiol.*, 2017, **8**, 108.
16 A. Postel, T. Letzel, S. Frischmann, C. Grund, M. Beer and T. Harder, *J. Vet. Diagn. Invest.*, 2010, **22**, 61–66.
17 W. Chen, B. He, C. Li, X. Zhang, W. Wu, X. Yin, B. Fan, X. Fan and J. Wang, *J. Med. Microbiol.*, 2007, **56**, 603–607.
18 Y. Xiang and Y. Lu, *Nat. Chem.*, 2011, **3**, 697–703.
19 L. Fu, J. Zhuang, W. Lai, X. Que, M. Lu and D. Tang, *J. Mater. Chem. B*, 2013, **1**, 6123–6128.
20 F. Hossain, N. Balasuriya, M. M. Hossain and M. J. Serpe, *Anal. Chem.*, 2022, **94**, 2056–2062.
21 L. Hou, C. Zhu, X. Wu, G. Chen and D. Tang, *Chem. Commun.*, 2014, **50**, 1441–1443.
22 F. Hossain, Q. Shen, N. Balasuriya, J. L. M. Law, M. Logan, M. Houghton, D. L. Tyrrell, M. A. Joyce and M. J. Serpe, *Anal. Chem.*, 2023, **95**, 7620–7629.
23 M. Eryilmaz, S. Ilbasmis-Tamer, S. Panhwar, E. K. Tayyarcan, I. H. Boyaci, Z. Suludere, D. Cetin, A. Zengin, E. Yildirim and U. Tamer, *Bioelectrochemistry*, 2025, **164**, 108936.
24 J. Hones, P. Muller and N. Surridge, *Diabetes Technol. Ther.*, 2008, **10**, S10–S26.
25 C. Nicolson, D. Major, J. M. Wood and J. S. Robertson, *Vaccine*, 2005, **23**, 2943–2952.
26 Y. Lee, I. Haizan, S. B. Sim and J.-H. Choi, *Sens. Diagn.*, 2024, **3**, 1124–1136.
27 K. H. Cha, G. C. Jensen, A. S. Balijepalli, B. E. Cohan and M. E. Meyerhoff, *Anal. Chem.*, 2014, **86**, 1902–1908.
28 Y. H. C. Leung, L. J. Zhang, C. K. Chow, C. L. Tsang, C. F. Ng, C. K. Wong, Y. Guan and J. S. M. Peiris, *Emerging Infect. Dis.*, 2007, **13**, 1380–1382.
29 C. Duan and R. Wang, *ACS Cent. Sci.*, 2024, **10**, 460–468.
30 M. D. de Jong, C. P. Simmons, T. T. Thanh, V. M. Hien, G. J. D. Smith, T. N. Chau, D. M. Hoang, N. V. Chau, T. H. Khanh, T. T. Dong, P. T. Qui, T. Cam, D. Q. Ha, Y. Guan, J. S. M. Peiris, N. J. White and J. Farrar, *Nat. Med.*, 2006, **12**, 1203–1207.
31 M. J. Pantin-Jackwood and D. E. Swayne, *Rev. Sci. Tech.*, 2009, **28**, 113–136.
32 R. A. Sheldon, *Chem. Soc. Rev.*, 2013, **42**, 6223–6235.
33 H. T. Tang, D. Norz, M. Grunwald, K. Giersch, S. Pfefferle, N. Fischer, M. Aepfelbacher, H. Rohde and M. Lutgehetmann, *J. Clin. Virol.*, 2024, **173**, 105693.
34 S. Ishii and M. J. Sadowsky, *Microbes Environ.*, 2008, **23**, 101–108.
35 H. M. Rowe, V. A. Meliopoulos, A. Iverson, P. Bomme, S. Schultz-Cherry and J. W. Rosch, *Nat. Microbiol.*, 2019, **4**, 1328–1336.
36 G. Younis, A. Awad, A. El-Gamal and R. Hosni, *Adv. Anim. Vet. Sci.*, 2016, **4**, 536–542.
37 W. C. Lee, M. C. Ho, S. W. Leu, C. C. Chang, C. K. Lin, C. M. Lin, Y. H. Fang, S. Y. Huang, Y. C. Lin, M. C. Chuang, T. M. Yang, M. S. Hung, Y. L. Chou, Y. H. Tsai and M. J. Hsieh, *J. Crit. Care*, 2022, **72**, 154164.
38 K. Jin, Z. Dai, P. Shi, Y. Li and C. Zhu, *BMC Infect. Dis.*, 2024, **24**, 31.
39 F. Krammer, E. Hermann and A. L. Rasmussen, *J. Virol.*, 2025, **99**, e0220924.
40 N. H. Martin, A. Trmcic and S. D. Alcaine, *JDS Commun.*, 2024, **5**, S4–S7.

41 S. Garg, C. T. Davis, R. T. Reed, E. A. Sleeman, J. R. Nolen, V. V. Tiwari, M. R. Reichert, J. C. McAllister, T. R. Stockwell, K. L. Johnson, L. M. Harris and R. B. Reed, *N. Engl. J. Med.*, 2025, **392**, 843–854.